Horizontal and Vertical Structure of Cross-Equatorial Wave Propagation

ROBERT A. TOMAS* AND PETER J. WEBSTER

Program in Atmospheric and Oceanic Sciences, University of Colorado, Boulder, Colorado

(Manuscript received 26 April 1993, in final form 28 October 1993)

ABSTRACT

Observational evidence of interhemispheric wave propagation through the equatorial upper-tropospheric mean westerlies in the eastern Pacific Ocean is found in nine years (1980/81 to 1988/89) of European Centre for Medium-Range Weather Forecasts analyses during boreal winter. Using time mean, standard deviation, and one-point correlation fields of potential vorticity on isentropic surfaces (IPV), it is found that waves associated with local fluctuations with periods between 6 and 30 days propagate from the Northern Hemisphere extratropics, cross the equator, and continue into the Southern Hemisphere extratropics. This result is in agreement with hypotheses that claim regions of time-mean westerlies in the tropics act as "ducts" allowing extratropical Rossby waves to propagate into and through the tropics.

Horizontal structure of the waves appears to change little during the course of the interhemispheric propagation. However, in the lower troposphere where the mean zonal wind is easterly, the lower portion of the extratropical waves do not cross the equator but stop and appear to dissipate locally. The horizontal structure of the lower-tropospheric waves changes dramatically when the waves encounter mean easterlies. Vertical one-point correlation analyses along the horizontal teleconnection path confirm the differential propagation with height when the waves reach the "easterly dome."

Linear theory is used to interpret the propagation characteristics of the waves and the changes in their horizontal and vertical structure as they encounter various mean flow distributions. It is suggested that during El Niño years, strong interhemispheric wave propagation may be observed in the eastern Atlantic region owing to an increase in the strength of the upper-level time-mean westerlies in that location. It is also suggested that the reverse phenomenon of wave propagation from the Southern Hemisphere into the Northern Hemisphere will most likely be observed when the westerly duct is open and the Southern Hemisphere midlatitudes act as a source of strong Rossby wave activity, such as during boreal fall.

1. Introduction

In an important note, Charney (1969) suggests that for Rossby waves with a meridional component of energy propagation, there may exist "critical latitudes" beyond which further north–south energy dispersion is not possible. Using simple linear arguments, he defines a critical latitude as the location where the time mean zonally averaged zonal wind component (i.e., $[\bar{u}]$, where the brackets and bar denote zonal and time averages) matches the zonal phase speed of the waves. This idea is an extension of Charney and Drazin (1961), who defined a similar constraint on the vertical propagation of planetary waves. In general, during winter, $[\bar{u}]$ decreases in magnitude in the troposphere and lower stratosphere as one moves from midlatitudes into the tropics, becoming easterly toward the equator. These observations led Charney to conclude that wave propagation between the midlatitudes and the tropics would be very limited because in the easterly regime it is possible only when the phase velocity of the disturbances is more easterly. As the energy in such ultralong extratropical waves is considered to be small, Charney concluded that the influence of extratropical modes on the tropics would be minimal. However, $[\bar{u}]$ is a strong a function of height as well as latitude so that it becomes only weakly easterly (or even weakly westerly, if one averages over selected time periods) at higher altitudes. Thus, Charney speculated that those disturbances that did propagate from middle latitudes into the tropics would tend to confine themselves to the high troposphere and lower stratosphere. In this way, he suggested the idea that vertical variations in the time-mean zonal wind may allow propagation between the extratropics and tropics.

Dickinson (1968a,b) considered the full vertical structure of $[\bar{u}]$. Using a simple numerical zonally averaged model, he showed it was possible for stationary extratropical waves to be routed vertically through the lower stratosphere at low latitudes. However, in line with Charney, he did not propose that these waves influenced tropical weather or that they propagated to the

* Current affiliation: National Center for Atmospheric Research, Boulder, Colorado.

Corresponding author address: Dr. Robert A. Tomas, NCAR, P.O. Box 3000, Boulder, CO 80307.

other hemisphere. Indeed, he postulated that the vertically and equatorward propagating waves would be absorbed in the strong stratospheric easterlies over the equator. Finally, given the sensitivity of the waves to their environment, it was assumed that the propagation characteristics of the waves would be greatly influenced by the phase of the quasi-biennial oscillation. However, the quasigeostrophic nature of the formulation precluded examination of this behavior close to the equator.

Charney and Dickinson had approached the problem of extratropical–tropical interaction from the viewpoint of a zonally averaged atmosphere. Thus, it was natural to think of the limit on meridional wave propagation as a critical latitude (or point) rather than as a "critical line" that may possess some kind of longitudinal structure. These arguments were rather pervasive and were used to justify the limitation of short-period forecast models to being hemispheric. Furthermore, within the confines of zonal symmetry or zonal averaging, Bates (1968), Mak (1970), and Webster (1973) basically confirmed Charney's conclusion that the tropical atmosphere was well insulated from extratropical disturbances by an effective critical latitude produced by the easterly wind regime.

However, the time-mean zonal wind field (i.e., $\bar{u}$) contains large zonal variations in the tropics, especially in the upper troposphere and lower stratosphere. The variations in $\bar{u}$ can be seen in Fig. 1, which shows the global winter mean (December through February) zonal wind on the 345-K isentropic surface (for reference, this surface resides fairly close to 200 mb; see Fig. 3). Although the winds are predominately easterly in the tropics, there are two regions of significant westerlies that span the equator. The stronger of the two, with a magnitude of order 20 m s^{-1}, is in the eastern Pacific and is about 7500 km wide. The weaker region of westerlies is in the eastern Atlantic and has a magnitude of about 5 m s^{-1} and is 4500 km wide. There is substantial annual and interannual variability in the strength of the equatorial westerlies. During boreal summer the westerlies almost disappear. During El Niño periods, the Pacific westerlies decrease to about 5 m s^{-1}, or almost disappear. On the other hand, the Atlantic westerlies increase in both size and magnitude and are similar to the normal conditions in the Pacific Ocean (Arkin and Webster 1985).

The extension of Charney's analysis to the case of a basic state that includes realistic meridional variations in $\bar{u}$ was made by Webster and Holton (1982). Using statistics for the upper troposphere compiled by Murakami and Unninayar (1977), they noted that maxima in the equatorial perturbation kinetic energy (PKE; the kinetic energy of motions with time scales less than the averaging period, in this case one month) occur where the time-mean zonal flow is westerly. This led Webster and Holton to speculate that the zones of time-mean westerlies in the equatorial upper tropical troposphere

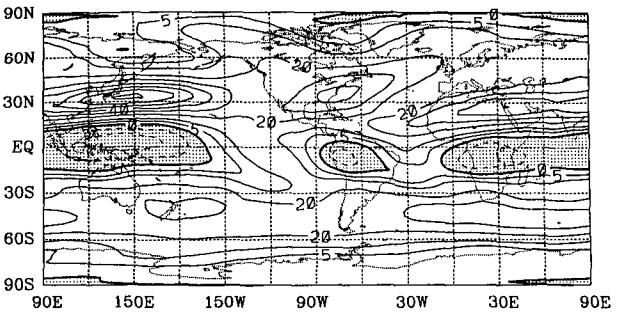

FIG. 1. The global DJF zonal wind on the 345-K surface. The contour interval is 10 m s^{-1} with the ± 5 m s^{-1} contours added. Regions where the wind is easterly are shaded and the $\bar{u} = 0$ contour is thickened.

act as ducts (termed "westerly ducts") that allow transient waves to propagate between extratropical and tropical regions or even into the other hemisphere. To test this hypothesis, Webster and Holton performed several experiments with a numerical formulation of a nonlinear shallow-water system. Similar to Charney, they found that stationary, global-scale, planetary waves are unable to propagate past a critical line where $\bar{u}$ vanishes. However, if the basic state includes a duct in which the zonal winds are westerly, waves of zonal scale less than the scale of the westerly duct may propagate from one hemisphere to the other. They also noted that the amplitude of the response in the hemisphere opposite the forcing increased strongly with the magnitude of the equatorial westerlies.

The observational component of this work was extended by Arkin and Webster (1985); using an 11-year record they note large spatial correlations between the time-mean zonal wind distribution and the PKE distribution in the tropics. They also note that the magnitude of the PKE increases as the time-mean zonal wind strength increases, adding to the evidence that motivated the earlier speculations by Webster and Holton. The analysis also showed that during warm events in the Pacific Ocean (i.e., El Niño periods) the locus of maximum variance shifts from the Pacific Ocean to the Atlantic following the maximum westerlies.

Until fairly recently, observational evidence of cross-equatorial teleconnections with time scales of less than one month has been rather scant. Blackmon et al. (1984a,b) studied teleconnections in fields of geopotential height during the Northern Hemisphere winter, including those resulting from fluctuations with periods between 10 and 30 days. They found wave trains propagating southward from midlatitudes. However, they did not seek evidence of cross-equatorial wave propagation as their analyses stopped at 20°N. Rather convincing evidence of the existence of interhemispheric teleconnections on time scales on the order of one to several weeks has been published very recently. Hsu and Lin (1992) investigated global tele-

connections during Northern Hemisphere winter using 10–30 day bandpass-filtered 250-mb streamfunction fields from the ECMWF analyses. They documented two that cross the equator, one passing through the Pacific westerly duct and another through the Atlantic Ocean counterpart. They noted that their findings are in agreement of the hypothesis with Webster and Holton (1982). Also, Kiladas and Weickmann (1992) investigated the influence of disturbances of midlatitude origin on tropical convection during the Northern Hemisphere winter using a technique that involves cross-correlating fields of outgoing longwave radiation (OLR) with upper-level National Meteorological Center (NMC) wind analyses. In fields made using 6–14 day bandpass-filtered data, they found evidence of a cross-equatorial teleconnection in the vicinity of the Pacific westerly duct.

In this paper, an interhemispheric teleconnection that crosses the equator through the Pacific westerly duct during Northern Hemisphere winter is also investigated. The signal is found in 6–30 day bandpass-filtered data, and we believe this is the same teleconnection pattern found by Hsu and Lin and Kiladas and Weickmann. However, the approach employed here differs from these previous studies, principally in three respects:

(i) The teleconnection is examined on several different levels, paying particular attention to the horizontal structure of the disturbances, the dependence of this structure on height, and its change along the teleconnection path. It is felt that the vertical dependence is very important since the time mean flow in the Pacific westerly duct varies considerably with height, from easterly at the surface to strongly westerly near the tropopause. The vertical variations in the time mean flow have a profound impact on wave propagation, in much the same way as the longitudinal variability (i.e., the presence or absence of the westerly ducts) does.

(ii) Details of the vertical structure of the disturbances are examined by constructing cross sections along the path of the teleconnection. This is particularly interesting because disturbances on this time scale tend to have a very deep (equivalent barotropic) structure in the midlatitudes but cannot maintain this depth during the course of their journey through the tropics because they must encounter the "easterly dome" in the lower troposphere.

(iii) Potential vorticity calculated on isentropic surfaces (usually termed isentropic potential vorticity or IPV) is chosen as the primary diagnostic variable.

In the second section we provide motivation for the choice of IPV, demonstrating that it is a useful tool for low-latitude diagnostics. The third section describes the data used in the study, the manner in which potential vorticity is calculated, and the statistical techniques used in rendering the data. The time mean characteristics in the vicinity of the Pacific westerly duct region are discussed in section 4. Transient features are also described in this section using IPV standard deviation fields and one-point correlation diagrams. Additionally, the vertical structure of cross-equatorial disturbance propagation is explored using a variation of one-point correlation technique along a vertical cross section. Section 5 attempts to explain the results in terms of the physical processes involved.

2. Utility of isentropic analysis in the tropics

The choice of the primary variable used in this study is motivated by several practical and theoretical considerations. The intuitive way in which many common meteorological phenomena (e.g., Rossby wave propagation; barotropic and baroclinic instabilities) may be interpreted and understood when viewed from an IPV perspective makes potential vorticity on an isentropic surface a particularly useful quantity for diagnostic work. This is a consequence of the familiar Lagrangian conservation principle and the so-called invertibility principle, which states formally that if the total mass under each isentropic surface is specified, then a knowledge of the global distribution of PV on each isentropic surface and of potential temperature at the lower boundary (along with a suitable balance condition) is sufficient to deduce all other dynamical fields, such as winds, temperatures, geopotential heights, static stabilities, and vertical velocities. These ideas are discussed extensively by Hoskins et al. (1985). For practical purposes, the invertibility principle can be summarized by several rules of thumb, which can be used to quickly determine, in a qualitative sense, the wind and thermal fields from a field of IPV. These rules are as follows.

(i) A positive (negative) IPV anomaly is associated with a positive (negative) vorticity anomaly.

(ii) In the NH, a positive (negative) IPV anomaly is associated with a positive (negative) static stability anomaly and negative (positive) static stability anomalies immediately above and below; the opposite is true in the SH.

(iii) The degree to which the flow associated with an anomaly penetrates upward and downward is proportional to the Coriolis parameter and, inversely, the static stability.

Given fields of IPV, it is a straightforward matter to qualitatively determine the wind field using the first rule, then apply the conservation principle and, to first order, interpret the time evolution in terms of the advection of IPV.

There are other good reasons for choosing IPV for the investigation of variance at low latitudes, especially when compared with the use of geopotential height on isobaric surfaces. To demonstrate the utility of IPV, a direct comparison of IPV and geopotential height is made; Figs. 2a–c show the zonal wind, geopotential height, and IPV in the horizontal domain 45°N to 45°S,

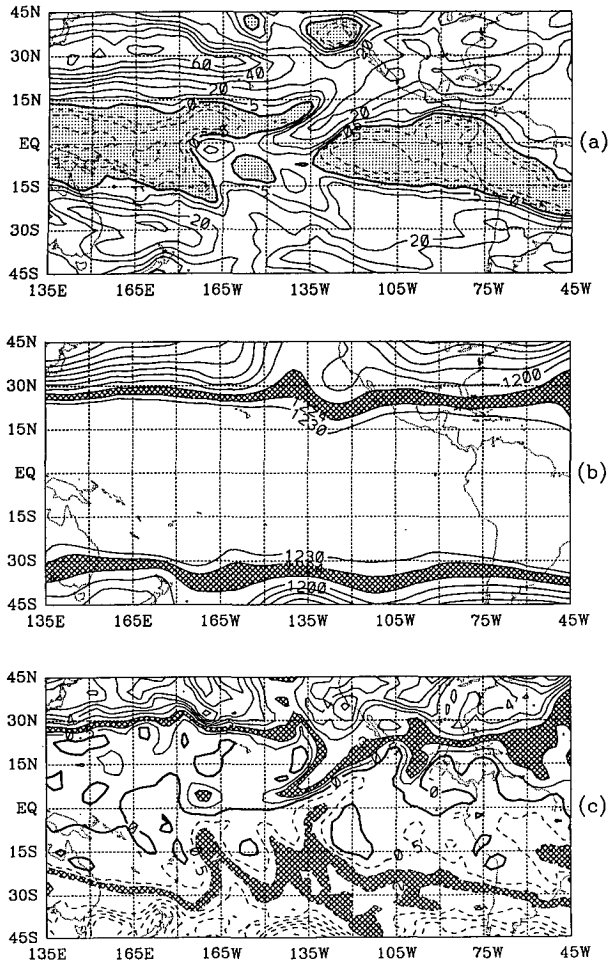

FIG. 2. (a) The zonal wind on the 345-K surface on 3 February 1984 for a region centered on the Pacific westerly duct. The contour interval is 10 m s^{-1} with the ± 5 m s^{-1} contours added. Regions where the wind is easterly are shaded. (b) The 200-mb geopotential height on the same day. The contour interval is 120 m with the 12 330 m contour added; the interval between 12 240 m and 12 120 m is cross-hatched. (c) The potential vorticity on the same day. The contour interval is 1.0×10^{-6} K m^2 (kg s)$^{-1}$ with the ± 0.5 unit contours added; the interval between 1.0×10^{-6} and 2.0×10^{-6} units is cross-hatched.

135°E to 45°W on 3 February 1984. The domain was chosen as it is centered on the Pacific Ocean westerly duct, which can be seen in the mean state (Fig. 1) or on the particular day (Fig. 2a). Figure 2b shows the 200-mb geopotential height distribution. With the exception of a "trough" protruding toward the equator along 135°W, the tropics are featureless. There is little evidence of transient behavior in the westerly duct or the existence of other tropical phenomena. The potential vorticity distribution on the 345-K isentropic surface (Fig. 2c) shows evidence of considerable activity, on the other hand. There are three major features apparent in the figure:

(i) Large areas of the tropics north of the equator, especially in the region of the westerly duct, contain negative IPV values. This indicates that, in the absence of processes that generate IPV, advection has occurred across the equator from the Southern Hemisphere. Positive values also occur in the Southern Hemisphere indications of the reverse propagation; for example, at 120°W and between the equator and 15°S there is a large area of positive IPV. The positive IPV extends just about as far into the Southern Hemisphere as the negative IPV extends into the Northern Hemisphere. However, the major excursions occur only in the immediate vicinity of the westerly duct.

(ii) Within the westerly duct, a tongue of positive IPV extends from about 30°N to the equator near 145°W. In the Southern Hemisphere there are two tongues of negative IPV extending equatorward from higher latitudes. The tongues in both hemispheres indicate excursions or propagations from higher latitudes. This is clear by following the hatched regions, which signify negative and positive IPV values between 1.0 and 2.0×10^{-6} units. Given the conservative nature of IPV, it is evident that there is substantial advection from higher latitudes.

(iii) The tilt of the IPV contours from northeast to the southwest indicate southward energy dispersion. Although the point will be discussed at greater length some time later, the orientation indicates that the two hemispheres are coupled through the westerly duct by wave propagation.

Another virtue of using IPV for tropical analysis can be drawn from comments made by Hsu and Lin (1992). They noted that the geopotential height field is not as suitable as the streamfunction or vorticity for teleconnectivity studies within a domain including both hemispheres. This is because in a quasigeostrophic system, the height anomalies tend to be positively correlated with the streamfunction in the Northern Hemisphere, but negatively correlated in the Southern Hemisphere. Thus, the signal of a wave train crossing the equator and composed of alternating cyclonic and anticyclonic circulation centers would be difficult to interpret in lagged one-point correlation fields formed using geopotential data.

Figure 3 shows the distribution of isentropes as a function of height (actually the logarithm of pressure) and latitude. As already noted, the 345-K surface resides very near to the 200-mb isobaric surface at all latitudes. Other isentropic surfaces show a very strong dependency on pressure and latitude. Our analysis considers horizontal variations on the 345-K and the 315-K surfaces. The vertical cross sections include data on other surfaces. It is worth noting that most isentropic surfaces intersect isobaric surfaces along a north–south cross section through the tropics. Although, at first glance, this may suggest that using isentropic surfaces may be undesirable, it will be demonstrated that they

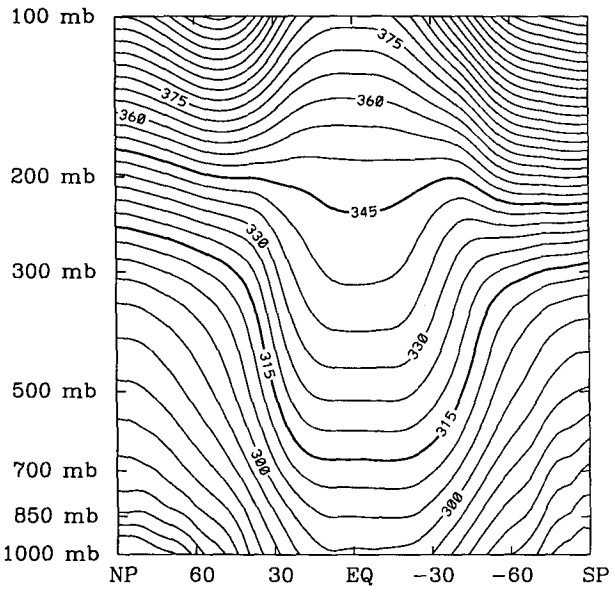

FIG. 3. The DJF zonally averaged potential temperature as a function of latitude and pressure. The contour interval is 5 K and the 345-K and 315-K contours are thickened.

are the best choice, not only because this results in PV being a conserved variable but also because the observations indicate that the disturbances tend to follow the isentropic surfaces rather than isobaric surfaces when the two diverge.

3. Data description and statistical analysis

a. The data

The European Centre for Medium-Range Weather Forecasts/World Meteorological Center (ECMWF/WMO) Global Analysis Data Sets are used for this study. They were made available by the National Center for Atmospheric Research (NCAR). These data are global in extent and represent initialized analyses at 00 Z and 12 Z. They include upper-air gridpoint fields for six physical parameters (geopotential height, temperature, horizontal wind components, vertical pressure velocity, and relative humidity) at each of seven standard pressure levels. The data are on a 2.5° × 2.5° latitude–longitude grid at pressure levels 1000, 850, 700, 500, 300, 200, and 100 mb. The period covered is from 1 January 1980 to 31 December 1989, inclusive.

Data representing the nine complete boreal winters (December, January, February: DJF) between 1980/81 and 1988/89 are used. A description and critique of the analyses during the period 1980–86 can be found in Trenberth and Olson (1988). Their greatest criticism was that during the early part of this period, the analyses resolved the divergent component of the wind poorly. However, since in calculating IPV the primarily concern is with the rotational part of the wind, this problem would seem to be of little consequence.

The winter mean fields are defined by

$$\bar{\alpha} = \frac{1}{9}\sum_{I=1}^{9}\frac{1}{90}\sum_{N=1}^{90}\alpha_{I,N}, \tag{1}$$

where I represents the year number ($I = 1$ represents the winter of 1980/81, etc.) and N represents the day number of winter ($N = 1$ represents 1 December of year I). The variance of α is given by

$$\alpha'^2 = \frac{1}{9}\sum_{I=1}^{9}\frac{1}{90}\sum_{N=1}^{90}(\alpha_{I,N} - \bar{\alpha})^2 \tag{2}$$

and the standard deviation by

$$\sigma(\alpha) = \sqrt{\alpha'^2}. \tag{3}$$

b. The calculation of potential vorticity on isentropic surfaces

The potential vorticity for large-scale flow is given

$$\Pi(p) = -g(\nabla_p \times \mathbf{V} + f\mathbf{k})\cdot\nabla_p\theta, \tag{4}$$

where $\Pi(p)$ is the potential vorticity on an isobaric surface, g is the gravitational acceleration, ∇_p is the 3D gradient operator, $\mathbf{V}$ is the horizontal velocity vector, f is the Coriolis parameter, $\mathbf{k}$ is the vertical unit vector, and θ is the potential temperature (Hoskins et al. 1985). Neglecting the product of the horizontal vorticity components with their respective horizontal temperature gradients yields the simplified expression for synoptic-scale flow (Burger 1991):

$$\Pi(p) = -g(\zeta + f)\frac{\partial\theta}{\partial p}. \tag{5}$$

The vertical component of relative vorticity, ζ, was calculated at each pressure level from the u and v components. The vertical gradient of potential temperature was estimated using a centered-difference scheme at intermediate levels and forward or backward schemes at boundary levels. The $\Pi(p)$ values were then linearly interpolated to the 315-K and 345-K isentropic levels yielding $\Pi(\theta)$ or IPV.

c. One-point correlations and filtering

One-point correlation analysis has been demonstrated to be an extremely useful tool for locating and analyzing teleconnections (e.g., Blackmon et al. 1984a,b; and many others). The method is to take a time series at one point in the field, called the base grid point, and to correlate it with all other points in the field. The correlation may be expressed as

$$\rho(\alpha_{x_1}, \alpha_{x_2}, \tau)$$

$$= \frac{1}{9} \sum_{I=1}^{9} \sum_{N=1}^{90} \frac{(\alpha_{x_2}, \tau - \overline{\alpha_{x_1}})(\alpha_{x_1}, \tau - \overline{\alpha_{x_2}})}{\sigma(\alpha_{x_1})\sigma(\alpha_{x_2})}, \quad (6)$$

where ρ is the correlation between the variable α at positions x_1 and x_2 at time lag τ.

If the fluctuations at the base grid point are associated with spatially coherent features, such as a wave train, the resulting correlation patterns will show alternating positive and negative centers. From such diagrams, one can determine the wavelength and the three-dimensional structure of the associated disturbances. By lagging and/or leading the fluctuations at all other points with respect to those at the base grid point, the time-dependent behavior of the waves can be studied. For example, it is possible to determine information about the phase and group velocity of the wave packet.

Before computing one-point correlation fields, the data were filtered in time to isolate the phenomena of interest. The twice daily IPV fields were first filtered using a 2-day low-pass tangential Butterworth filter developed by Kaylor (1977), and the sampling rate was reduced to once daily in order to reduce the volume of data. Before filtering, the time mean was removed. The 2-day low-pass data were subsequently filtered with 6-day and 30-day low-pass filters. The response curves of the filters are shown in Fig. 4. Bandpass data containing fluctuations with periods between 6 and 30 days were formed by subtracting the appropriate low-pass fields. The 6-day cutoff was chosen because the results of Blackmon et al. (1977) and others have shown that local fluctuations with periods less than 6 days include the signal of midlatitude, transient disturbances that propagate rapidly in the zonal direction. Lower-frequency fluctuations contain the signal of more slowly moving disturbances (which have been interpreted as Rossby waves propagating on a sphere) and are of interest here because they frequently possess a significant component of meridional propagation. The 30-day cutoff was chosen to remove the signal of more slowly varying phenomena, which have been shown to be associated with quasi-stationary teleconnections (Blackmon et al. 1984a,b). Several other considerations were also taken into account when making this decision. Some case studies of wave propagation across the equator in this region were examined and it was noted that the disturbances produced local fluctuations with periods of about 10 to 15 days. Also, power spectra calculated at grid points to the northwest of the duct contained several peaks within this frequency range.

To estimate the significance of correlations between the base grid point and all other field points, the time scale, T, between two independent points is defined by

$$T = 1 + \sum_{\tau=-\infty}^{+\infty} \rho(\alpha_{x_1}, \alpha_{x_1}, \tau), \rho(\alpha_{x_2}, \alpha_{x_2}, \tau)\Delta t, \quad (7)$$

where $\rho(\alpha_{x_1}, \alpha_{x_1}, \tau)$ and $\rho(\alpha_{x_2}, \alpha_{x_2}, \tau)$ are the biased autocorrelations at time lag τ for base grid point x_1 and field point x_2 and Δt is the sampling interval, 1 day. The summation was limited to lags between ± 40 days because the filtering removed over 95% of the power from periods longer than this. The degrees of freedom (DOF) can then be estimated by

$$\text{DOF} = \frac{N\Delta t}{T}, \quad (8)$$

where N is the number of records (e.g., Hsu and Lin 1992). The DOF at every grid point for the base grid point located at 22.5°N, 165°W were calculated. For the 345-K data, the minimum DOF was 76, and for the 315-K data, the minimum was 69. Thus, each point has at least 60 DOF and this value was used, for convenience, in a Student's t-test. To reject the null hypothesis of no correlation between two points, at the 90% level correlations must exceed 0.17, at the 95% level they must exceed 0.21, and at the 99% level they must be greater than 0.30. The correlations emphasized in the discussions that follow all exceed 0.20. In addition, we believe that the spatially coherent nature of the patterns lends to their interpretation as real physical phenomena rather than random correlations.

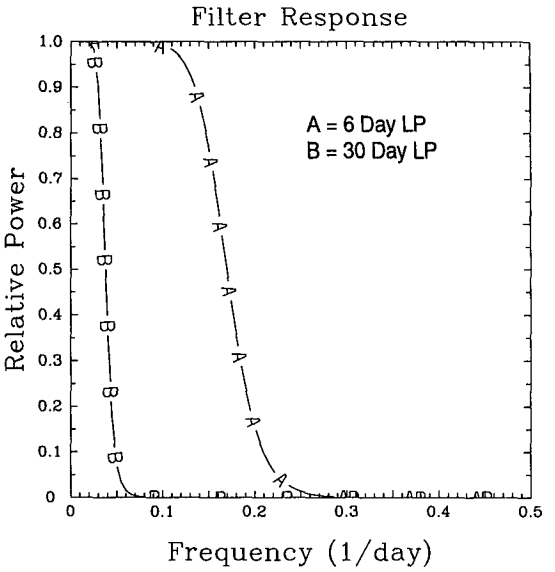

FIG. 4. The filter response functions. Curve (A) is for the 6-day low pass and curve (B) is for the 30-day low pass.

4. Structure of the time mean fields

In this section the structures of the wintertime mean IPV, $\bar{u}$, and $\bar{v}$ on the 345-K and 315-K isentropic surfaces are discussed. These mean fields are very important as they represent the basic states upon which the transient fluctuations are superimposed, at least to the extent that WKBJ linear theory is valid. Figures 5 and 6 show the fields for the two isentropic surfaces.

Figure 5a shows the 345-K DJF mean IPV field. For the most part, values are positive in the Northern Hemisphere and negative in the Southern Hemisphere. However, on the 345-K surface, the zero contour does not exactly coincide with the equator with small positive and negative mean IPV departures extending into the Southern and Northern Hemispheres, respectively. In addition, in the Northern Hemisphere, a trough of high IPV extends equatorward near 135°W, and northward of this feature there is a "ridge." Taken together, these two features constitute a split flow pattern in the eastern Pacific. The protrusion of extratropical values of IPV into the tropics occurs in the vicinity of the westerly duct, as can be seen in Fig. 5b. Regions of upper-tropospheric easterlies are shaded in this figure. The Pacific westerly duct, with wind speeds between 10 and 20 m s^{-1}, is the most striking feature at low latitudes. It spans the tropics, providing a swath of continuous westerlies connecting the Northern Hemisphere and Southern Hemisphere midlatitudes. The duct tilts from the northwest to the southeast and extends from just east of the Hawaiian islands to just west of the South American coast. Outside the duct region the flow is easterly with maximum values of greater than −10 m s^{-1} over Indonesia.

The meridional gradient of IPV is largest in the midlatitudes off the east coast of Asia and to a lesser extent, off the east coast of North America. These tight gradients correspond to the two strong jets in the Northern Hemisphere seen in Fig. 5b. The jet off the Asian coast shows speeds in excess of 70 m s^{-1}, while the North American jet exceeds 40 m s^{-1} in the mean. An interesting feature is the asymmetry of the SH, low-latitude trough in the IPV field. The asymmetry occurs in the east–west direction, with the trough decaying more abruptly to the west than to the east. Furthermore, the region of maximum westerly wind within the duct slopes from the northwest to the southeast.

The $\bar{v}$ on the 345-K surface is shown in Fig. 5c. In the Northern Hemisphere subtropics there is a dipole pattern 180° out of phase with a similar pattern in midlatitudes. The quadrupole in this field is consistent with the split flow pattern seen in the IPV field. In the Southern Hemisphere extratropics, there is a dipole pattern that is consistent with the trough in the IPV field. In the tropics, there are northerlies coincident with the westerly duct even at the equator. Thus, the time-mean flow in the westerly duct region of the Pacific Ocean has both westerly and northerly components. The southerlies are much weaker than the westerlies, however, being an order less in magnitude.

The character of the fields on the lower-level 315-K surface is in sharp contrast to those just shown. Overall, the IPV field (Fig. 6a) is rather flat and featureless in both hemispheres, with the exception of the weak ridge off the west coast of the United States. Larger IPV values occur only near the northern boundary of the domain. Clearly, there are large differences between the time-mean flow regimes at these different levels, especially at the lower latitudes.

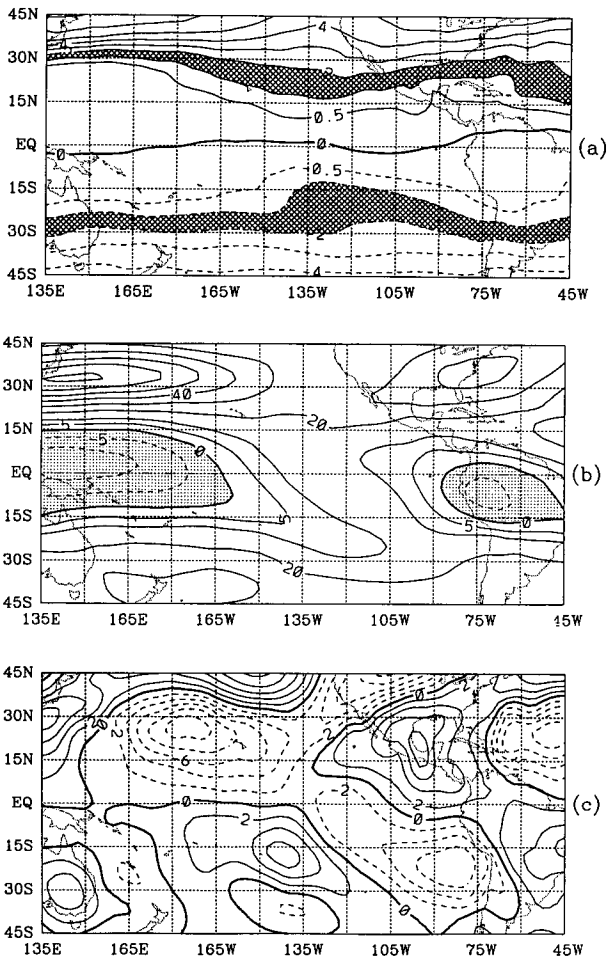

FIG. 5. (a) The DJF 345-K IPV. The contour interval is 1.0×10^{-6} K m^2 $(kg\ s)^{-1}$ with the ±0.5 unit contour added; the interval between 1.0×10^{-6} and 2.0×10^{-6} units is cross-hatched. (b) The DJF 345-K zonal wind. The contour interval is 10 m s^{-1} with the ±5 m s^{-1} contours added. Regions where the wind is easterly are shaded and the $\bar{u} = 0$ contour is thickened. (c) The DJF 345-K meridional wind. The contour interval is 2 m s^{-1}. The $\bar{v} = 0$ contour is thickened.

Figure 6b shows uninterrupted easterlies in the tropics from the western to eastern edge of the domain with maximum values between −5 and −10 m s^{-1}. These extensive easterlies represent the greatest change between the 345-K and 315-K levels. That is, at the 315-K level, a westerly duct is not apparent and the mean zonal wind component is dominated by the vertical extension of easterlies into the midtroposphere. In the midlatitudes of the Northern Hemisphere, the jets off the east coasts of Asia and North America are still present but are weaker and positioned slightly poleward of those at the upper level. The Southern Hemisphere field has little meridional structure. The 315-K level $\bar{v}$ (Fig. 6c) is relatively smooth except for the midlatitudes of

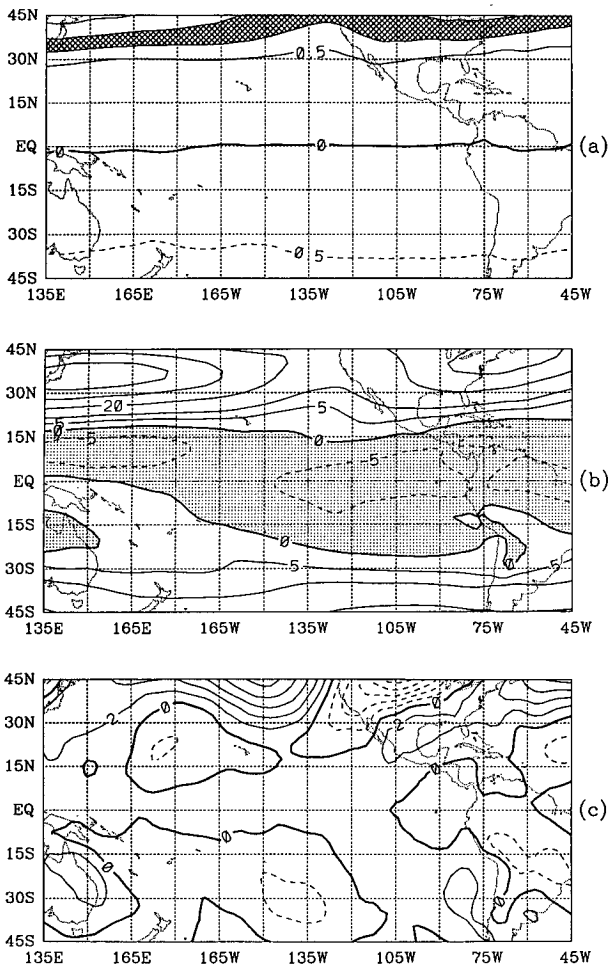

FIG. 6. (a) The DJF 315-K IPV. The contour interval is 1.0×10^{-6} K m^2 (kg s)$^{-1}$ with the ± 0.5 unit contour added; the interval between 1.0×10^{-6} and 2.0×10^{-6} units is cross-hatched. (b) The DJF 315-K zonal wind. The contour interval is 10 m s^{-1} with the ± 5 m s^{-1} contours added. Regions where the wind is easterly are shaded and the $\bar{u} = 0$ contour is thickened. (c) The DJF 315-K meridional wind. The contour interval is 2 m s^{-1}. The $\bar{v} = 0$ contour is thickened.

Northern Hemisphere. The quadrupole, so evident at 345 K (Fig. 5c), has been replaced by a zonally oriented dipole near 45°N, which straddles the stationary ridge in the IPV field off the west coast of North America.

5. Structure of the transients

In order to examine the higher-order statistics or transients in the IPV, a number of statistical quantities were calculated: specifically, standard deviation fields and horizontal and vertical one-point correlations fields. These are discussed in the following paragraphs.

a. Standard deviation fields

The standard deviation of the IPV on the 345-K and 315-K surfaces were calculated using the bandpass-filtered data and the results of the analysis are shown in Figs. 7a–b. The two figures show striking differences. Whereas a local maximum spans the equator in the region of the westerly duct on the 345-K surface, the entire tropical belt is featureless on the 315-K surface. Larger values at 315-K are confined to the midlatitudes of both hemispheres and the field has fewer and weaker features in comparison with the upper-level surface. Largest values are found poleward of the time mean ridge and, to a lesser extent, equatorward of the trough off the west coast of North America. Throughout the tropics, values remain quite low. Only in the regions of mean tropical easterly winds are there low values of variance on the 345-K surface.

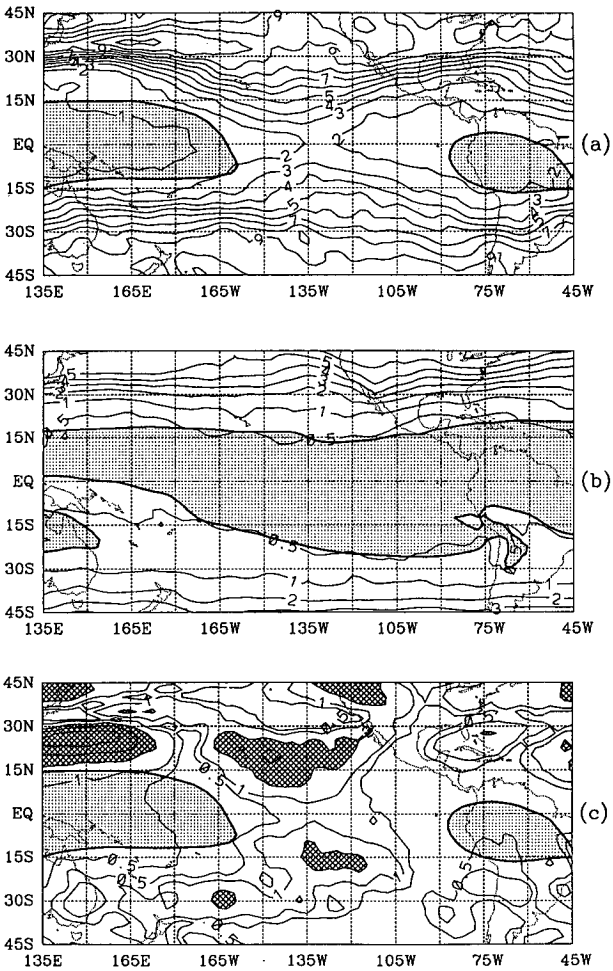

FIG. 7. (a) The DJF 345-K 6–30 day IPV standard deviation. The contour interval is 1.0×10^{-6} K m^2 (kg s)$^{-1}$. The $\bar{u} = 0$ contour is included and regions where the wind is easterly are shaded. (b) The DJF 315-K 6–30 day IPV standard deviation. The contour interval is 1.0×10^{-6} K m^2 (kg s)$^{-1}$. The $\bar{u} = 0$ contour is included and regions where the wind is easterly are shaded. (c) The DJF 345-K 6–30 day IPV standard deviation with the zonal mean removed. The contour interval is 1.0×10^{-6} K m^2 (kg s)$^{-1}$. The $\bar{u} = 0$ contour is included, and regions where the wind is easterly are shaded.

On the 345-K surface, largest standard deviation values are associated with two zonally elongated features located in the Northern Hemisphere midlatitudes between 30° and 45°N. One elongation extends from the east coast of Asia to the west coast of the United States and the other extends eastward from the east coast of North America. These maxima correspond to the main Northern Hemisphere storm tracks (e.g., Blackmon et al. 1984a). Although not shown, it is found that the strength of these two maxima increases and they are displaced slightly poleward if fluctuations with time scales less than 6 days are included. The effect of the split flow is apparent by the way the western Pacific IPV standard deviation maximum conforms to both the poleward and equatorial sides of mean IPV "block-like" structure (Fig. 5a). In the Southern Hemisphere, there is a zonally symmetric storm track southward of 40°S or to the poleward side of the simpler mean zonal wind maximum.

A careful comparison of the time mean (Fig. 5) and standard deviation fields (Fig. 7) reveals that the large, southward extrusion of fluctuations from the Northern Hemisphere extratropics is located slightly westward of the time-mean trough. This displacement suggests that disturbances propagate along the *western* and *southern* edges of this feature. In the Southern Hemisphere, there is a northward extrusion of high standard deviation values into the tropics located just east of its Northern Hemisphere counterpart. Being located slightly eastward of the Southern Hemisphere trough, it has a different relationship with the local time-mean field, suggesting that here disturbances propagate along the *northern* and *eastern* edges of the trough. In Fig. 7c the zonal mean has been removed in order to elucidate this point. Now it is clearer that the largest departures from zonal symmetry lie along the western edge of the time mean trough in the Northern Hemisphere and along the eastern edge of the trough in the Southern Hemisphere, consistent with the notion that the fluctuations are a result of disturbances propagating from the NH into the SH where the background (time mean) flow structure is most favorable.

b. *Horizontal one-point correlation fields*

One-point correlation fields were made at various lags using the bandpass-filtered data. The primary results presented are with the base grid point located at 22.5°N, 165°W. This correlation base point was chosen as it produces the strongest cross-equatorial response at upper levels. However, any point in the general vicinity yields similar results, albeit slightly weaker.

Figures 8a–c show one-point correlations using data on the 345-K surface with fluctuations in the field lagging those at the base grid point by 3 days, simultaneous to, and leading those at the base grid by 3 days, respectively. The correlations refer to fluctuations relative to the mean structures discussed in Fig. 5. Regions

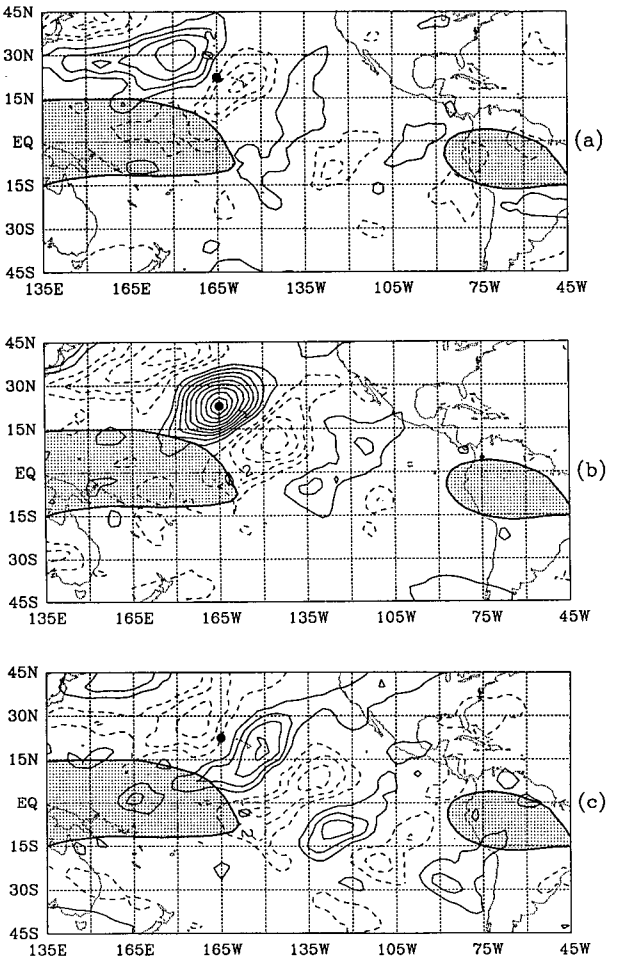

FIG. 8. One-point correlation fields formed using the DJF 345-K 6–30 day IPV. The base grid point is located at 22.5°N, 165°W. (a) Field points lag the base grid point by 3 days. (b) Field points lag by 0 days (simultaneous). (c) Field points lead by 3 days.

where the time mean zonal wind is easterly have been shaded and the base grid point (22.5°N, 165°W) is marked with a heavy dot. In the 3-day lag panel (Fig. 8a), a wave train originates in the Northern Hemisphere midlatitudes, extends southward into the Northern Hemisphere tropics and crosses the equator through the westerly duct. In the simultaneous panel (Fig. 8b), the correlations at the base grid point and the regions immediately downstream from the base grid point, increase in strength. Three days later (Fig. 8c), correlation values at these centers decrease. However, values increase at locations farther downstream, suggesting energy propagation into the Southern Hemisphere. Correlation centers that appear to be part of a coherent wave train extend into the Southern Hemisphere to near 30°S.

Attention is drawn to several aspects of these correlation centers. First, they are tilted such that their major axis is aligned from northeast to southwest, which

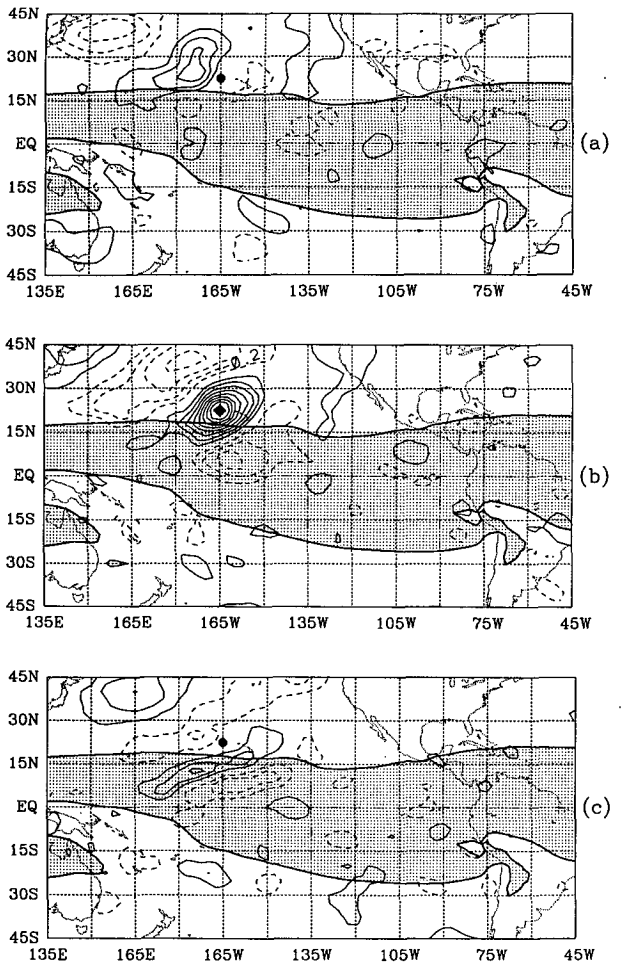

FIG. 9. One-point correlation fields formed using the DJF 315-K 6–30 day IPV. The base grid point is located at 22.5°N, 165°W. (a) Field points lag the base grid point by 3 days. (b) Field points lag by 0 days (simultaneous). (c) Field points lead by 3 days.

is consistent with disturbances having a southward energy flux. Second, the longitudinal scale of the centers is smaller than the scale of the westerly duct and it appears that they are able to propagate through the region unimpeded by critical surfaces. The phase velocity of the waves can be estimated using this figure. In the zonal direction, correlation centers move about 15 degrees every 3 days, which corresponds to about 6 m s^{-1}. In the meridional direction, they move at about half this speed, about 3 m s^{-1}. Furthermore, local correlation centers change sign every 6 days; thus, the waves are associated with local fluctuations with a period of about 12 days.

A rough estimate of the relative strength of the disturbances at the equator compared to the strength of those in the midlatitude can be made using Fig. 7a. The IPV standard deviation values near the base grid point are between 7 and 8 units and at the equator they are between 2 and 3 units, or about 30% as strong.

Figures 9a–c show the same one-point lagged correlations but on the 315-K surface. In the −3 day panel (Fig. 9a), the correlation centers upstream of the base grid point, in the midlatitudes, resemble those seen at the 345-K level. There is no evidence, however, of spatially coherent correlations downstream extending across the equator. In the simultaneous correlation field (Fig. 9b), the centers appear markedly different than those at the upper level, especially those downstream of the base grid point. The correlation center immediately downstream of the base grid point is positioned nearly due southward and there are no others located farther downstream. In the +3 day panel (Fig. 9c), all correlations have weakened and those in the tropics have become elongated in the zonal direction and compressed in the meridional direction. The orientation of the major axes of the centers, nearly east–west, is indicative of the physical processes occurring at the lower level. The significance of the change in shape will be discussed in the next section.

In order to determine whether these waves are a significant source of wave activity in the tropics and the SH, we made one-point correlation maps with the base grid point located on the equator at 127.5°W and in the SH at 10°S, 112.5°W. If the waves contribute significantly to the local variance, we expect to see a wave train similar to the one in Fig. 8.

Figures 10a–b show the results for the equatorial base grid point at lags of −2 and +1 days, respectively.

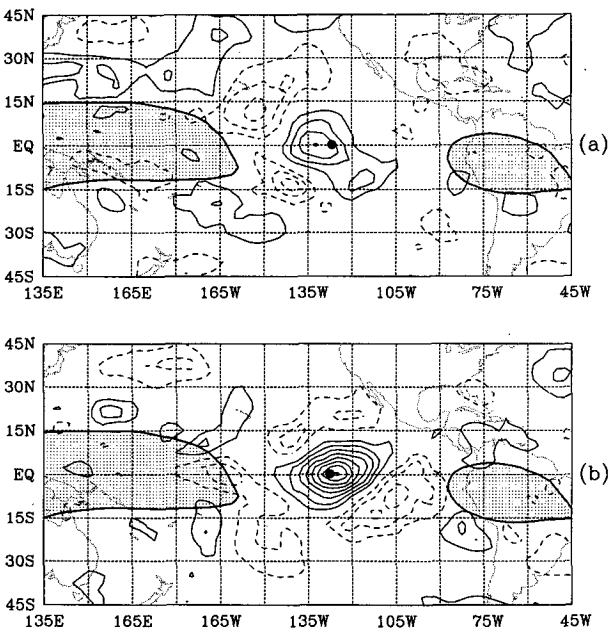

FIG. 10. One-point correlation fields formed using the DJF 345-K 6–30 day IPV. The base grid point is located at the equator, 127.5°W and is marked with a heavy dot. The contour interval is 0.1 and the zero contour is omitted. (a) Field points lag the base grid point by 2 days. (b) Field points lead by 1 day.

In the −2 day lag figure, there is a wave train extending back into the NH midlatitudes similar to the one in Fig. 8a. Interestingly, there are also correlation centers extending back (southwestward) into the SH, suggesting that wave energy emanating from *both* hemispheres is associated with local fluctuations at the equator in the Pacific westerly duct.

The corresponding +1 day lag figure shows the stronger correlation centers in the SH; they alternate between positive and negative values and form a wave train similar to that seen in Fig. 8c. It appears that little energy makes it way into the NH from the SH, however, as the correlation centers in the NH do not suggest a similar wave train propagating in the opposite direction.

The analogous results with the base grid point located at 10°S, 112.5°W (Figs. 11a–b) show a wave train much like those seen in Figs. 8a–c and Figs. 10a–b. In the −2 day panel (Fig. 11a), the stronger correlation centers are in the NH, while in the +1 day panel (Fig. 11b), they are in the SH.

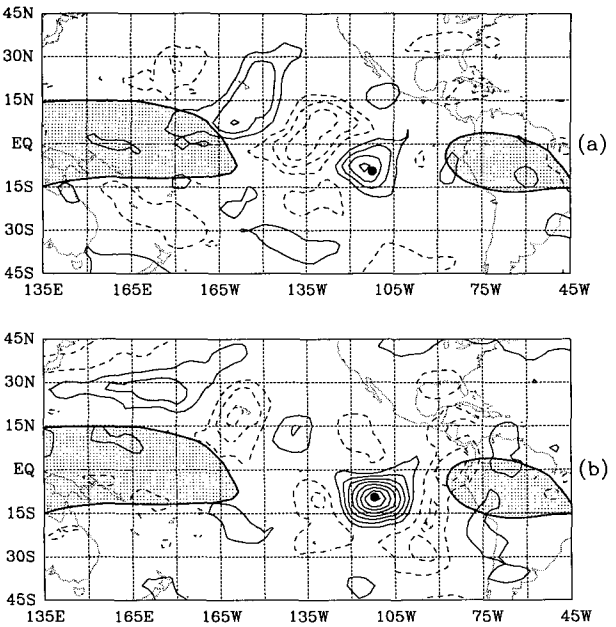

FIG. 11. One-point correlation fields formed using the DJF 345-K 6–30 day IPV. The base grid point is located at 10°S, 112°W and is marked with a heavy dot. The contour interval is 0.1 and the zero contour is omitted. (a) Field points lag the base grid point by 2 days. (b) Field points lead by 1 day.

c. *Vertical one-point correlation fields*

In order to better examine the vertical structure of the interhemispheric teleconnection pattern, one-point correlation fields were made using vertical cross-sectional data. The horizontal extent of the cross section was chosen by drawing a line through the wave train that appears in the one-point correlation field on the 345-K surface at lag +3 days (Fig. 8c) from its origin in the Northern Hemisphere midlatitudes to its termination in the Southern Hemisphere midlatitudes. The resulting line runs from 45°N, 160°E to 45°S, 60°W, includes the base grid point, and passes through all the correlation centers. In order to maximize vertical resolution, the potential vorticity data calculated on all seven pressure levels is used. The base grid point is located at 22.5°N, 165°W and 200 mb. The time mean isentropes have been superimposed (dashed lines) together with the zero mean zonal wind contour (heavy solid curve). The zero mean wind contour represents the top of the easterly dome. Figures 12a–c show those results for field points with lags of −3, 0, and +3 days.

In the −3 day lag panel, there are alternating positive and negative correlation centers extending from the Northern Hemisphere midlatitudes into the Southern Hemisphere tropics. There are three large correlation centers in the Northern Hemisphere: a negative center near 45°N, labeled A, a positive center near 30°N, labeled B, and another negative center near 15°N, labeled C; two lesser centers in the Southern Hemisphere have been labeled D and E.

Centers A and B have a dipole structure in the vertical. Since the disturbances at these latitudes undoubtedly maintain the same direction of rotation throughout their depth, the static stability anomaly must change sign somewhere in the lower troposphere. This is consistent with the rule of thumb for diagnosing such information from IPV fields (Hoskins et al. 1985). The height of the nodal line between positive and negative poles moves downward between centers A and B, suggesting that the disturbances tend to follow the isentropic surfaces rather than the pressure surfaces. As the disturbances encounter the time mean easterlies (centers D and E), the lower portion of these correlation centers seems to be restrained, causing them to tilt slightly forward with height. Thus, where the wave encounters the $\bar{u} = 0$ line, propagation is inhibited. The disturbance do penetrate slightly into the easterlies, but only where the easterlies are weak.

In the simultaneous correlation field, centers A, B, and C have all moved approximately 7.5 degrees equatorward. The node between positive and negative poles for centers A and B moves downward during the process, while C has lifted and rides over the dome of easterlies. Finally, the centers D and E are weaker and are located higher in the atmosphere.

In the +3 day panel the individual centers have all moved 7.5 degrees farther equatorward, and a continuous wave train stretches from the Northern Hemisphere to the Southern Hemisphere. Again, the bottom portion of the disturbances appears to be "held back" in the presence of the easterly dome in the lower troposphere of the tropics. The interhemispheric wave train is confined to the upper troposphere southward of the easterly dome. The correlation centers tend to re-

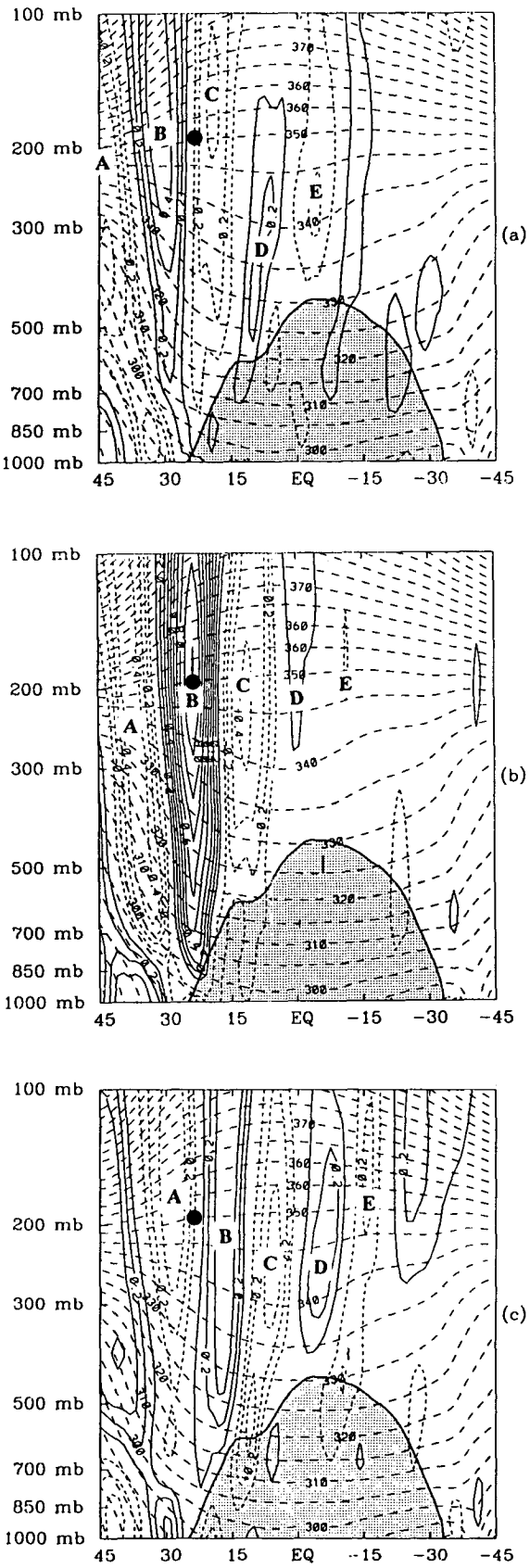

main exclusively upper-level features even after they have entered the Southern Hemisphere, although by rule of thumb (iii), we might expect downward penetration as the disturbances move away from the equator. Perhaps some weak indication of this exists near 30°S where there is a weak vertical dipole of the type seen in the Northern Hemisphere midlatitudes. The lower correlation is quite weak, however, and this interpretation must be made cautiously.

6. Discussion

The results in the last section show strong evidence of midlatitude Rossby wave activity propagating through the westerly duct region. To analyze the structure of the waves and to interpret the observations, WKBJ linear theory is used. In addition to the assumption that the dynamics are linear, further simplifications will be made in order to keep the arguments readily tractable. Specifically:

(i) The time-mean meridional wind is assumed to be zero. Although it was shown that there is a southerly component to the mean wind in the duct region at upper levels, its magnitude is an order less than the zonal component.

(ii) The zonal wind is taken to be a function of latitude only. This assumption is justified when the waves under consideration are of a smaller zonal scale than the westerly duct, as seems to be the case for the waves seen in the upper-level, one-point correlation fields (Figs. 8a–c). Put another way, if the duct is wide enough to allow the waves to pass through unimpeded, then increasing the width of the duct would not change this result. Conversely, if the waves encounter a region of easterlies sufficiently broad to prohibit further meridional propagation, increasing the meridional extent of the easterlies will not change this result either.

(iii) In the same spirit as in (ii), equations are used that describe barotropic flow. In doing so, it is implicitly assumed that the vertical structure of the time mean and eddy variables can be accounted for by considering the total flow to be composed of several separate barotropic layers. This approach may be justified by noting that the vertical one-point correlation results (Figs. 10a–c) show that as the deep, equivalent barotropic midlatitude disturbances propagate through the westerly duct, the lower portion is left behind although the upper part continues to propagate. The upper-level disturbances that remain appear have a structure that is

FIG. 12. Vertical one-point correlation fields formed using the DJF 6–30 day IPV along a line from 45°N, 160°E to 45°S, 60°W. The base grid point is located at 22.5°N, 165°W, 200 mb. The contour interval is 0.1 and the zero contour is omitted. (a) Field points lag the base grid point by 3 days. (b) Field points lag by 0 days (simultaneous). (c) Field points lead by 3 days.

nearly barotropic. Thus, it would appear that the basic structure is unchanged although there are substantial changes in the equivalent depth of the mode.

The results of the analysis can only have qualitative value because of the linear assumption, but it will be shown that in spite of all these simplifications, the theoretical relationships derived are consistent with the observations, demonstrating that considerable, qualitative insight can be gained using this highly simplified approach.

The dispersion relation for barotropic flow is given by

$$\omega = \bar{u}k - \frac{\beta^* k}{(k^2 + l^2 + f_0^2/c^2)}, \tag{9}$$

where ω is the modal frequency, $\bar{u}$ the time mean zonal wind speed, k the zonal wavenumber, β^* the meridional gradient of the Coriolis parameter plus the gradient of the vorticity associated with the mean flow, $-(\partial^2\bar{u}/\partial y^2)$, l the meridional wavenumber, f_0 the Coriolis parameter, and $c^2 = gH$, where g is the gravitational acceleration and H is the equivalent depth of the disturbances. To obtain the meridional group speed, c_{g_y}, (9) is differentiated with respect to l, yielding

$$c_{g_y} = \frac{\partial\omega}{\partial l} = \frac{2\beta^* kl}{(k^2 + l^2 + f_0^2/c^2)^2}, \tag{10}$$

which can be simplified by using the zonal phase velocity, obtained from (7) as

$$c_{p_x} = \frac{\omega}{k} = \bar{u} - \frac{\beta^*}{(k^2 + l^2 + f_0^2/c^2)}. \tag{11}$$

Solving (11) for l^2 gives

$$l^2 = \frac{\beta^*}{(\bar{u} - c_{p_x})} - k^2 - \frac{f_0^2}{c^2}, \tag{12}$$

which with (10) yields

$$c_{g_y} = \frac{2kl(\bar{u} - c_{p_x})^2}{\beta^*}. \tag{13}$$

Equations (12) and (13) can be interpreted in the following way:

(i) As long as the time-mean zonal wind speed is greater than the zonal phase speed of the waves, meridional energy dispersion is possible.

(ii) If the time-mean zonal wind speed approaches the zonal phase speed, however, the meridional energy dispersion should decrease and eventually cease. This is a direct consequence of (13), which shows that c_{g_y} goes to zero as $(\bar{u} - c_{p_x})$ goes to zero.

(iii) As a consequence of (12), l^2 must increase if a wave train approaches a critical line.

Clearly, Figs. 8a–c demonstrate that the observations are consistent with the notion that eastward moving waves are able to propagate across the equator where the time-mean flow is eastward at a greater speed as suggested by (i) above. The estimated zonal phase speed of the disturbances of about 7 m s^{-1} is well less than the 10 to 20 m s^{-1} observed in the duct (Fig. 5a). On the other hand, from Fig. 6b, the time mean zonal wind speed on the 315-K surface below the westerly duct is -5 m s^{-1} and the interpretation described in (ii) applies. Furthermore, Figs. 9a–c show that although the waves do penetrate somewhat into the easterlies, the waves do not cross the equator through the easterly dome. Perhaps not too surprisingly, the waves at the lower level in the tropics behave quite differently than their upper-level counterparts as they are controlled by the very different basic state within which they find themselves.

The anomalous behavior of the waves on the lower isentropic surfaces can be seen from another perspective in the vertical one-point correlation fields (Figs. 12a–c). As the wave train moves southeastward out of the midlatitudes, the disturbances appear to be moving along isentropic surfaces, but this progress is hindered as they encounter the easterly dome. The movement of the lower part of the disturbances slows and there is little development of correlation centers farther downstream. However, the upper part of the disturbances, above the easterly dome, continues to move through the westerly duct as is evidenced by the well-defined upper-level wave train present in the +3 day panel.

During this study, one-point correlation fields were calculated using other base grid points. In all cases examined, midlatitude wave trains effectively penetrate into the tropics only where the time mean zonal wind is westerly. During the Northern Hemisphere winter, penetration was found in the westerly ducts of both the eastern Pacific and eastern Atlantic. However, it should be noted that the time mean zonal wind in the Atlantic duct is generally considerably weaker than observed in the Pacific (Fig. 1). Correspondingly, the cross-equatorial teleconnection signal was found to be much weaker. The variation of the strengths of the teleconnection patterns is in keeping with the observations of Arkin and Webster (1985), who showed that variance in the westerly ducts is strongly dependent upon the strength of the westerlies. They noted, as well, that during an El Niño the upper-tropospheric westerlies in the eastern Pacific decrease substantially or are absent entirely but the Atlantic westerly duct increases in magnitude substantially. Although the hypothesis has not been tested at this time, Atlantic teleconnection patterns should be of greatest magnitude during an El Niño. On the other hand, maximum amplitude wave trains should occur in the Pacific sector during the opposite phase of an El Niño, namely, the La Niña.

Another aspect of the wave behavior is consistent with the theoretical arguments described above. On the 315-K surface (Figs. 9a–c), the meridional wavelength of the disturbances decreases from about 45 de-

grees in the midlatitudes to 15 degrees in the tropics. This is consistent with (12), which indicates that l should increase as the wave train approaches the critical line as indicated in item (iii).

7. Concluding remarks

The results presented in this study strongly suggest that interhemispheric teleconnections on time scales from about a week to a month are a real facet of the Northern Hemisphere wintertime circulation in the upper troposphere of the eastern Pacific. Teleconnections were found in fields of IPV on the 345-K surface derived from ECMWF analyses. The features of the pattern appear to be similar to that found by Hsu and Lin (1992) using 250-mb ECMWF streamline fields and Kiladas and Weickmann (1992) using cross correlations between OLR and the NMC wind analyses.

It is also clear that while the disturbances are quite deep in the extratropics, only the upper portion of the disturbance, that part above the easterly dome, is able to propagate across the equator. While moving through the Northern Hemisphere midlatitudes, the disturbances seem to follow the isentropic surfaces rather than the pressure surfaces. In the tropics the lower isentropic surfaces intersect the easterly dome and further southeastward propagation appears to be hindered, in agreement with the theoretical arguments presented.

Strong westerlies are observed in the Pacific duct region from October until May. Since it appears that the interhemispheric response depends primarily on the strength of the local westerlies at the equator, as was suggested by Webster and Holton (1982), it seems logical to extend this work to include other months. For example, during the NH fall, we feel it is most likely that wave propagation from SH into the NH may be observed since the SH circulation is still quite vigorous and located farther equatorward, having not fully made the transition to warm season pattern conditions.

Acknowledgments. The authors wish to thank Dr. Hai-Ru Chang for providing valuable technical assistance during the course of this research. The European Centre for Medium-Range Weather Forecasts analyses were made available by the National Center for Atmospheric Research. This study was supported by the Atmospheric Science Division of the National Science Foundation under Grants ATM-87-03267 and ATM-92-14840.

REFERENCES

Arkin, P. A., and P. J. Webster, 1985: Annual and interannual variability of tropical–extratropical interaction. *Mon. Wea. Rev.*, **113,** 1510–1523.

Bates, J. R., 1970: Dynamics of disturbances on the intertropical convergence zone. *Quart. J. Roy. Meteor. Soc.*, **96,** 677–701.

Blackmon, M. L., 1976: A climatological spectral study of the 500 mb geopotential height of the Northern Hemisphere. *J. Atmos. Sci.*, **33,** 1607–1623.

——, Y.-H. Lee, and J. M. Wallace, 1984a: Horizontal structure of 500 mb height fluctuations with long, intermediate and short time scales. *J. Atmos. Sci.*, **41,** 961–979.

——, ——, and ——, 1984b: Time variation of 500 mb height fluctuations with long, intermediate and short time scales as deduced from lag-correlation statistics. *J. Atmos. Sci.*, **41,** 981–991.

Branstator, G., 1983: Horizontal energy propagation in a barotropic atmosphere with meridional and zonal structure. *J. Atmos. Sci.*, **40,** 1689–1708.

Burger, A. P., 1991: The potential vorticity equation: from planetary scale to small scale. *Tellus,* **43A,** 191–197.

Charney, J. G., and P. G. Drazin, 1961: Propagation of planetary-scale disturbances from the lower into the upper atmosphere. *J. Geophys. Res.*, **66,** 83–109.

——, 1969: A further note on large-scale motions in the tropics. *J. Atmos. Sci.*, **26,** 182–185.

Dickinson, R. E., 1968a: On the exact and approximate linear theory of vertically propagating planetary Rossby waves forced at a spherical lower boundary. *Mon. Wea. Rev.*, **96,** 405–415.

——, 1968b: Planetary Rossby waves propagating vertically through weak westerly wind wave guides. *J. Atmos. Sci.*, **25,** 984–1002.

——, 1970: Development of a Rossby wave critical level. *J. Atmos. Sci.*, **27,** 627–633.

Hoskins, B. J., M. E. McIntyre, and A. W. Robertson, 1985: On the use and significance of isentropic potential vorticity maps. *Quart. J. Roy. Meteor. Soc.*, **111,** 877–946.

Hsu, H.-H., and S.-H. Lin, 1992: Global teleconnections in the 250-mb streamfunction field during the northern winter. *Mon. Wea. Rev.*, **120,** 1169–1190.

Kaylor, R. E., 1977: Filtering and decimation of digital time series. Technical Note BN850, Inst. Phys. Sci. Tech., University of Maryland, College Park, MD, 42 pp.

Kiladas, G. N., and K. M. Weickmann, 1992: Extratropical forcing of tropical Pacific convection during northern winter. *Mon. Wea. Rev.*, **120,** 1924–1938.

Mak, M. K., 1969: Laterally driven stochastic motions in the tropics. *J. Atmos. Sci.*, **26,** 41–64.

Murakami, T. M., and M. S. Unninayar, 1977: Atmospheric circulation during December 1970 through February 1971. *Mon. Wea. Rev.*, **105,** 1024–1038.

Trenberth, K. E., and J. G. Olson, 1988: Inter-comparison of the NMC and ECMWF global analyses: 1980–1986. NCAR/TN-301+STR Technical Note, National Center for Atmospheric Research, Boulder, CO, 81 pp.

Webster, P. J., 1973: Remote forcing of the time-independent tropical atmosphere. *Mon. Wea. Rev.*, **101,** 58–68.

——, and J. R. Holton, 1982: Cross-equatorial response to middle-latitude forcing in a zonally varying basic state. *J. Atmos. Sci.*, **39,** 722–733.